AFRL-ML-WP-TP-2006-488

ULTRASONIC DETECTION USING CORRELATION IMAGES (PREPRINT)

Raini Cepel, K.C. Ho, Brett A. Rinker, Donald D. Palmer, Jr., and Steven P. Neal

AUGUST 2006

Approved for public release; distribution is unlimited.

STINFO COPY

MATERIALS AND MANUFACTURING DIRECTORATE
AIR FORCE RESEARCH LABORATORY
AIR FORCE MATERIEL COMMAND
WRIGHT-PATTERSON AIR FORCE BASE, OH 45433-7750

REPORT DOCUMENTATION PAGE

Form Approved
OMB No. 0704-0188

1. REPORT DATE *(DD-MM-YY)*	2. REPORT TYPE	3. DATES COVERED *(From - To)*
August 2006	Conference Paper Preprint	01/01/2005 – 12/31/2005

4. TITLE AND SUBTITLE
ULTRASONIC DETECTION USING CORRELATION IMAGES (PREPRINT)

5a. CONTRACT NUMBER
FA8650-04-C-5704

5b. GRANT NUMBER

5c. PROGRAM ELEMENT NUMBER
62112F

6. AUTHOR(S)
Raina Cepel and K.C. Ho (University of Missouri-Columbia/Electrical and Computer Engineering)
Steven P. Neal (University of Missouri-Columbia/Mechanical and Aerospace Engineering)
Brett A. Rinker (Honeywell)
Donald D. Palmer, Jr. (The Boeing Company)

5d. PROJECT NUMBER
N/A

5e. TASK NUMBER
N/A

5f. WORK UNIT NUMBER
N/A

7. PERFORMING ORGANIZATION NAME(S) AND ADDRESS(ES)

University of Missouri-Columbia
Mechanical and Aerospace Engineering
E3401 Lafferre Hall
Columbia, MO 65211

University of Missouri-Columbia
Electrical and Computer Engineering
Columbia, MO 65211

The Boeing Company
Phantom Works
St. Louis, MO

Honeywell Federal Manufacturing and Technology
Kansas City, MO

8. PERFORMING ORGANIZATION REPORT NUMBER

9. SPONSORING/MONITORING AGENCY NAME(S) AND ADDRESS(ES)
Materials and Manufacturing Directorate
Air Force Research Laboratory
Air Force Materiel Command
Wright-Patterson AFB, OH 45433-7750

10. SPONSORING/MONITORING AGENCY ACRONYM(S)
AFRL-ML-WP

11. SPONSORING/MONITORING AGENCY REPORT NUMBER(S)
AFRL-ML-WP-TP-2006-488

12. DISTRIBUTION/AVAILABILITY STATEMENT
Approved for public release; distribution is unlimited.

13. SUPPLEMENTARY NOTES
This work, resulting in whole or in part from Department of the Air Force contract FA8650-04-C-5704, has been submitted to the American Institute of Physics for publication in the Proceedings of the 2006 33rd Annual Review of Progress in Quantitative Nondestructive Evaluation (QNDE 2006).

This is the best quality of this paper available. PAO Case Number: AFRL/WS 06-2142, 5 Sep 2006.

14. ABSTRACT
In ultrasonics, image formation and detection are generally based on signal amplitude. In this paper, we describe an amplitude independent approach for imaging and detection based on the similarity of adjacent signals, quantified by the correlation coefficient calculated between A-scans. Correlation coefficient images are introduced and shown with C-scan images to demonstrate flat-bottom-hole and crack detection in experimental data and planar defect detection at very low signal-to-noise ratio using simulated data. ROC analysis compares the new correlation method and the classical method.

15. SUBJECT TERMS
ultrasonics, signal processing, correlation, crack detection, weld inspection, flaw detection

16. SECURITY CLASSIFICATION OF:			17. LIMITATION OF ABSTRACT:	18. NUMBER OF PAGES	19a. NAME OF RESPONSIBLE PERSON (Monitor)
a. REPORT	b. ABSTRACT	c. THIS PAGE			Gary Steffes
Unclassified	Unclassified	Unclassified	SAR	14	19b. TELEPHONE NUMBER *(Include Area Code)* N/A

Standard Form 298 (Rev. 8-98)
Prescribed by ANSI Std. Z39-18

ULTRASONIC DETECTION USING CORRELATION IMAGES

Raina Cepel,[1] K. C. Ho,[1] Brett A. Rinker,[3] Donald D. Palmer, Jr.,[4] and Steven P. Neal[2]

[1] Electrical and Computer Engineering
[2] Mechanical and Aerospace Engineering
University of Missouri-Columbia, Columbia, MO 65211
[3] Honeywell Federal Manufacturing and Technology, Kansas City, MO
[4] The Boeing Company, Phantom Works, St. Louis, MO

ABSTRACT. In ultrasonics, image formation and detection are generally based on signal amplitude. In this paper, we describe an amplitude independent approach for imaging and detection based on the similarity of adjacent signals, quantified by the correlation coefficient calculated between A-scans. Correlation coefficient images are introduced and shown with C-scan images to demonstrate flat-bottom-hole and crack detection in experimental data and planar defect detection at very low signal-to-noise ratio using simulated data. ROC analysis compares the new correlation method and the classical method.

Keywords. ultrasonics, signal processing, correlation, crack detection, weld inspection, flaw detection
PACS. 43.20.Hq, 43.20.Ye, 43.20.-f, 43.35.Cg

INTRODUCTION

The most common method of flaw detection in ultrasonic nondestructive evaluation is based on C-scan images. One weakness of this peak-amplitude dependent method its sensitivity to background noise, especially at low signal-to-noise ratio (SNR) where false-positive and false-negative detection rates may be unacceptably high. In this paper we present a complimentary approach that relies on the similarity between adjacent A-scans with the assumption that flaw signals change shape less quickly as the transducer changes position than do noise signals. The amount of shape change present is quantified by the correlation between adjacent windowed A-scans. [1-3]

This paper will discuss the issues involved with correlation imaging and provide example correlation images for both measured and simulated data. Computer generation of noise and statistical performance analysis are also addressed.

DATA

Ultrasonic data was collected in immersion mode from three samples. The first sample was a stainless steel plate. A Panametrics 10 MHz, ½" diameter, 4" focal length transducer at normal incidence was used to collect grain noise signals over a regular 45 x

62 grid with 0.5 mm between measurement positions. This data was used for showing example noise correlation images and its statistical properties were used for the creation of simulated noise. The second sample was a stainless steel annular ring with an inside diameter of 40 mm and an outside diameter of 70 mm which was machined to add five equal depth flat bottomed holes. This sample was scanned at normal incidence with a Panametrics 15 MHz, ½" diameter, 6" focal length transducer over a polar grid with 2^0 between radial scan lines and 0.762 mm between circumferential scan lines. The third sample was comprised of two aluminum plates fastened together. EDM notches were machined between select fastener locations. Oblique incidence pitch-catch measurements were made using two Panametrics 10 MHz ½" transducers (one focused and one planar) arranged 5^0 from normal. Data from these two samples was used to demonstrate the correlations analysis for various flaw types and for both polar and Cartesian scans.

Data was also simulated to provide a means of controlling SNR and defect region size. This data, *x*, was created by adding a simulated defect signal, represented as a Gaussian damped sinusoid, *y*, scaled by *B*, to simulated grain noise, *n,* at each *ij* position.

$$x(i,j,t) = n(i,j,t) + B(i,j)y(t) \tag{1}$$

The defect mask matrix *B(i,j)* can be spatially varied to create flaws with varied size, positioning, and SNR. A defect mask image is shown in the results section.

Simulated grain noise signals were generated to match both the maximum extreme value (gated peak value) distribution and the correlation coefficient distribution obtained from the measured grain noise. [4] The simulation procedure is beyond the scope of this paper, but the basic process involves creating each A-scan as a weighted sum of the adjacent A-scans and a random component with the weights chosen to create the desired correlation between the new and adjacent signals.

THE CORRELATION APPROACH

Calculations

The statistic of interest is the spatial cross-correlation coefficient calculated between two A-scans adjacent in position. Consider an *N x M* scan with each A-scan *T* points long where the matrix $\mathbf{x} = x(i,j,t)\ \ i = 1...N\ \ j = 1...M\ \ t = 0...T-1$ holds the data. Calculation of the correlation between A-scans is then given by the following equation where $\hat{\rho} = \hat{\rho}(i,j,\delta_r,\delta_c,\tau)$ is a sample estimate of the associated expected value: [5]

$$\hat{\rho} = \frac{\sum_{t=t_i}^{t_f}[x(i,j,t-\tau) - m_x(i,j)][x(i+\delta_c, j+\delta_r, t) - m_x(i+\delta_c, j+\delta_r)]}{\sqrt{\sum_{t=t_i}^{t_f}[x(i,j,t-\tau) - m_x(i,j)]^2}\sqrt{\sum_{t=t_i}^{t_f}[x(i+\delta_c, j+\delta_r, t) - m_x(i+\delta_c, j+\delta_r)]^2}} \tag{2}$$

where t is a discrete temporal index. Subtraction of the mean (m_x and m_y) of each signal along with the normalization removes the scale dependence and restricts $\hat{\rho}$ to the range -1 to 1. Row correlations and column correlations can be calculated with $\delta_r = 1,\ \delta_c = 0$ and $\delta_r = 0,\ \delta_c = 1$, respectively. In Eq. (2), the summation range in the time domain defines

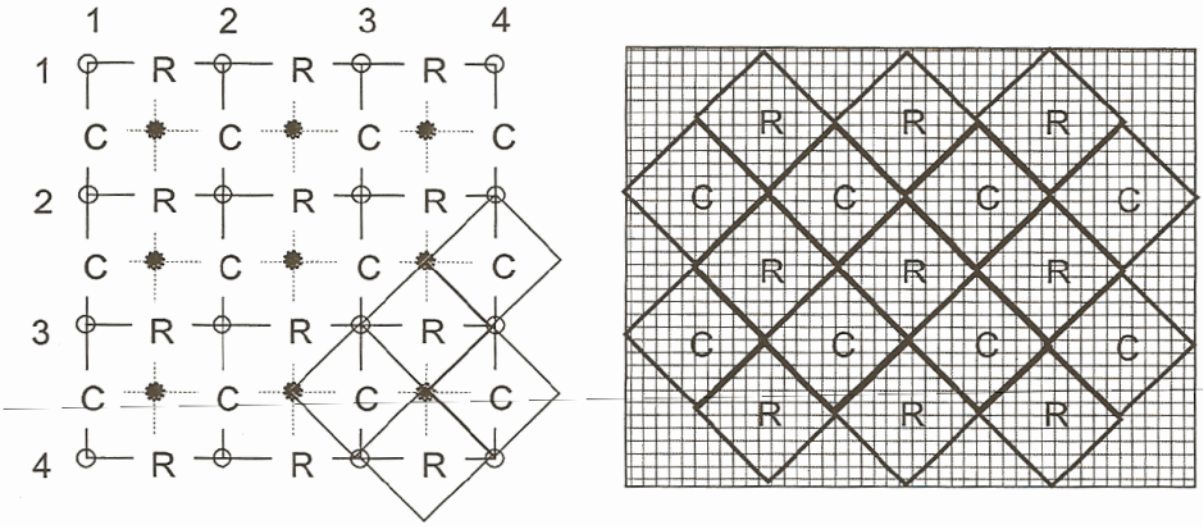

FIGURE 1. (a) Measurement positions are represented by open circles, row correlations by 'R', and column correlations by 'C', and blank positions by closed circles. (b) By considering each correlation as a diamond shaped element, a highly discretized matrix can be used for imaging.

the portion of the signal (the time window) of interest, τ controls the temporal shift between signals, and δ is a spatial shift parameter ($\delta = 1$ for adjacent measurement positions). For all calculations, τ was set to zero, assuming perfect alignment of defect signals; however, τ can be varied in Eq. (2) to achieve signal alignment.

Imaging

The issue of imaging row and column correlation coefficients is not simple, primarily because there are approximately twice as many correlation coefficients as measurement positions. For an N x M matrix, there are $N(M-1)$ row correlations and $(N-1)M$ column correlations, resulting in $2NM - M - N$ total correlations. Figure 1 shows a schematic representation of a 4 x 4 scan (left figure) with open circles at the 16 measurement positions. The R's and C's are used to represent the positions conceptually assigned to row and column correlations, respectively. A polar scan can be treated in similar fashion with the R's and C's representing the positions assigned to radial and circumferential correlations, respectively. For the 4 x 4 example, to maintain spatial registration, the 24 correlations coefficients can be written into a 7 x 7 matrix (see Fig. 1), leaving 25 blank elements. These blank elements spatially correspond to positions of the open and solid circles in the schematic. The easiest image formation approach is to make separate row and column correlation images. Another imaging solution is to assign each blank element an average of nearest neighbor values. An alternative approach which avoids smoothing is to shift the column correlations up one row. This approach compromises spatial registration; however, the resultant images are useful for qualitative evaluation. A final approach which preserves spatial registration is to consider each correlation value as being centered in a diamond-shape region (see Fig. 1). This approach can be applied to both Cartesian and polar scan data. To facilitate display of the diamond regions, a matrix with a much higher number of elements than the original correlation matrix is used to approximate the diamond-shaped regions, that is, the diamonds are discretized (see the right schematic in Fig. 1). Each element in the high density matrix is assigned a value based on which diamond that element falls within. The pixels outside of the diamond-filled regions are set to a single (arbitrary) value. Figure 2 shows example

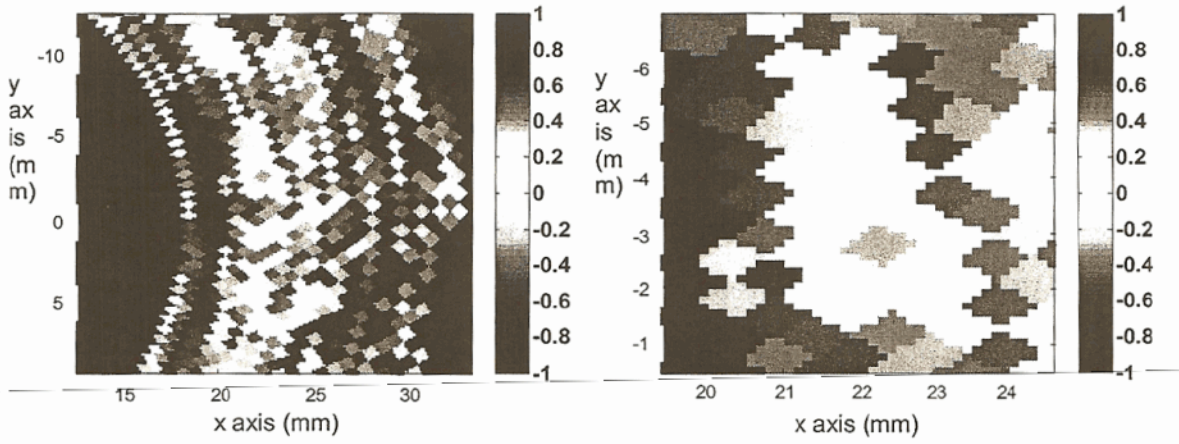

FIGURE 2. Correlation images using high discretization; (a) Cartesian scan and (b) polar scan.

images created with this method using data taken in both Cartesian (left image) and polar (right image) scans.

SIGNAL PROCESSING AND STATISTICAL ANALYSIS

Additional methods were used in the implementation and evaluation of the correlation approach. Thresholding was applied to provide a statistical basis for detection. Measurements made in a region known to be defect-free can be used to establish a distribution of correlation coefficients for grain noise. A detection threshold can then be chosen to control the false-positive rate based on the grain noise correlation coefficient distribution. A square moving-average window is used to reduce the variance in the grain noise correlation distribution. Averaging results in less overlap between the tails of the noise correlation distribution and the flaw correlation distribution (generally unknown), making defects easier to differentiate from noise. Square averaging windows were used in this work, but the shape of the averaging window can also be changed to detect differently shaped flaws. In order to improve detection over a range of defect size, ten averaging windows were applied to each image with the window size ranging from 1x1 to 10x10. For each averaging window size, thresholding was applied with a value of 1 was assigned to the corresponding threshold matrix if the threshold was exceeded and a value of 0 was assigned if the threshold was not exceeded. The 10 threshold matrices where then essentially added to create the final threshold image with pixel values ranging from 0 to 10. A value of 0 indicates no detection hits while a 10 indicates detection for all averaging window sizes. An analogous approach was used to create C-scan based threshold images.

Receiver operating characteristic (ROC) analysis can be used to quantify the separation between two distributions. Specifically, an ROC curve shows the true positive fraction (TPF) versus the false positive fraction (FPF) as the threshold is systematically varied. ROC curves can be calculated for correlation analysis and C-scan analysis under varying analysis conditions (SNR, averaging window size, etc.). The area under the ROC curve can be used as a basis for performance comparison across detection techniques and across analysis conditions. For very high SNR when the distributions are completely separated (Fig. 3(a)), the ROC curve is ideal (Fig. 3(b)), and the area under the ROC curve is unity. At lower SNR when the distributions overlap (Fig. 3(c)), the ROC curve (Fig. 3(d)) reflects the tradeoff between TPF and FPF (false-detection), and the area under the curve is less than one. Initial ROC analysis results are shown in the next section.

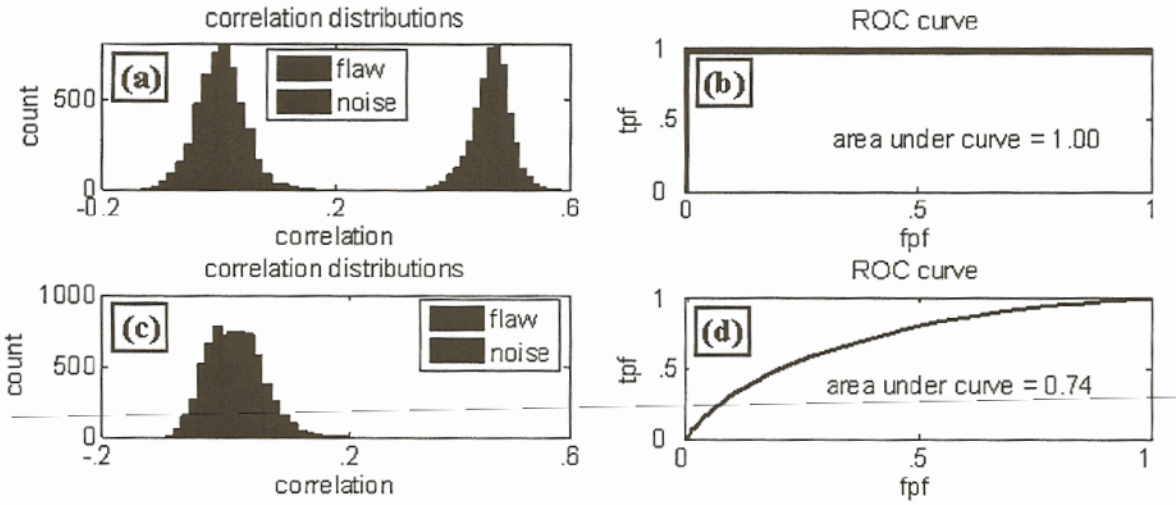

FIGURE 3. ROC curves (right) from two different sets of distributions (left).

RESULTS

Results for the annular stainless steel ring are shown in Figure 4 with the C-scan image on the left and the correlation image on the right. High values in the innermost and outermost diameters are due to multiple reflected signals from features not in the plane of the defects and can be ignored. Starting from the top and moving clockwise, there are three 1/16", one 2/16", and one 3/16" flat-bottom holes. In both images, all holes are visible; however, for the smaller holes the contrast between the flat-bottom-hole region and the background noise is greater for the correlation image.

Figure 5 shows the results for the aluminum sample. The sample was scanned in pitch-catch mode and consists of two aluminum plates fastened together as depicted in Fig. 5(a). EDM notches were machined between the fasteners as shown in Fig. 5(b). Because the sample was scanned in pitch-catch, the presence of a fastener or notch results in a loss of signal peak-amplitude in the C-scan image (Fig. 5(c)) and low correlation values in the correlation image (Fig. 5(d)). The three longer notches are easily detected in both images. This example demonstrates defect detection based on a reduction in correlation relative to a defect-free region.

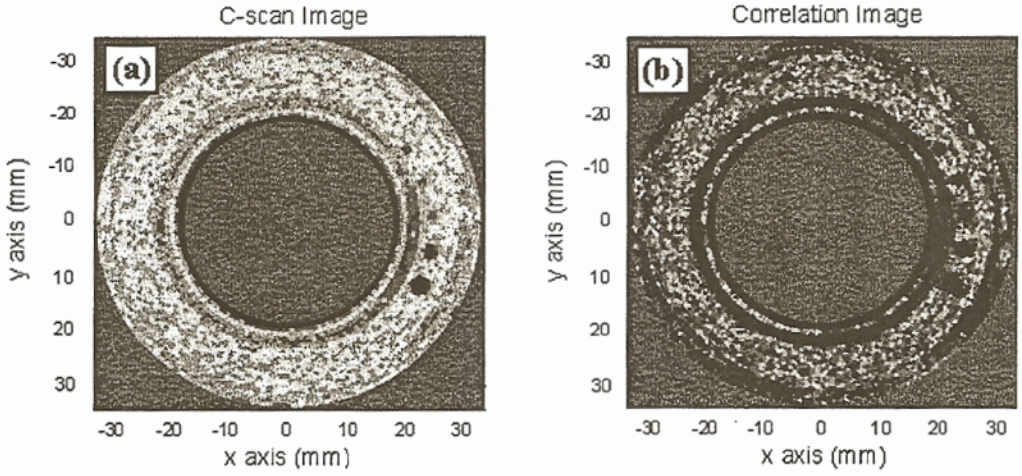

FIGURE 4. Images of annular stainless steel ring; (a) C-scan and (b) correlation.

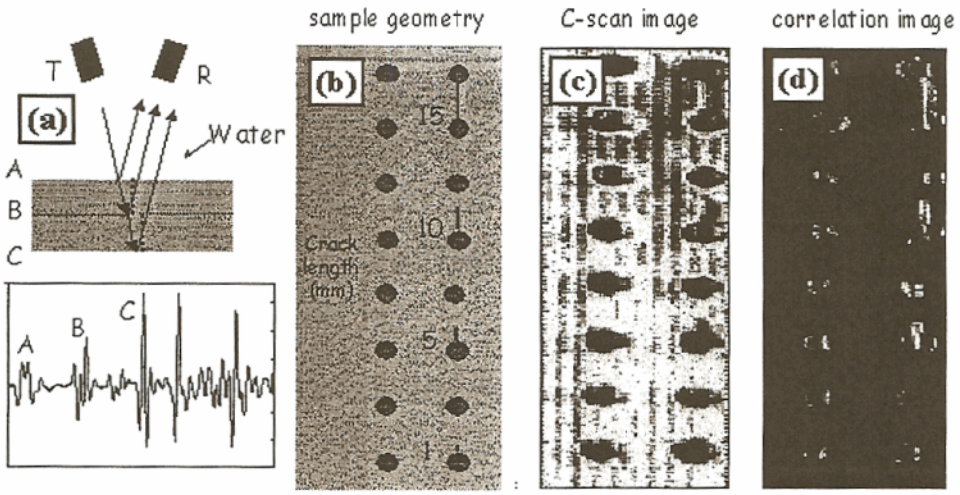

FIGURE 5. Scan of aluminum sample; (a) set-up, (b) flaws locations (c) C-scan, and (d) correlation image.

Figure 6 shows the results for a set of simulated data. Five flaws were created using the defect mask shown in the figure with SNRs in the range of 0.28-0.90. The C-scan image and C-scan threshold image allow detection of 4 of the defects. The correlation image reveals the same four flaws as well as a hint of the very low SNR flaw in the mid-upper right of the image. The correlation threshold image identifies all five defects. In this very low SNR simulation example, the correlation approach performs better than the classical C-scan approach in terms of both detection and sizing of defects.

Comparison of the performance of the correlation approach with classical C-scan and matched filter approaches is ongoing. In this section, we show only initial results comparing the correlation and C-scan approaches. Figure 7(a) shows the area under the ROC curve (SNR = 0.6) for both approaches plotted versus the measurement spacing between adjacent A-scans. For the C-scan approach, the area under the ROC curve remains relatively stable as the measurement spacing changes. For the correlation approach, as the measurement spacing increases, the mean of the noise correlation coefficient distribution tends toward zero, the defect correlation distribution shows minimal change, and correlation-based detection becomes more effective. Clearly, for the correlation approach to work, defect signals must be present at multiple measurement positions. For defects with relatively large lateral extent and low SNR, these results suggest that increasing the measurement spacing will increase the efficacy of the correlation approach. Figure 7(b) shows ROC area versus SNR. For both approaches, performance is better at a higher SNR. However, at a low SNR the correlation approach

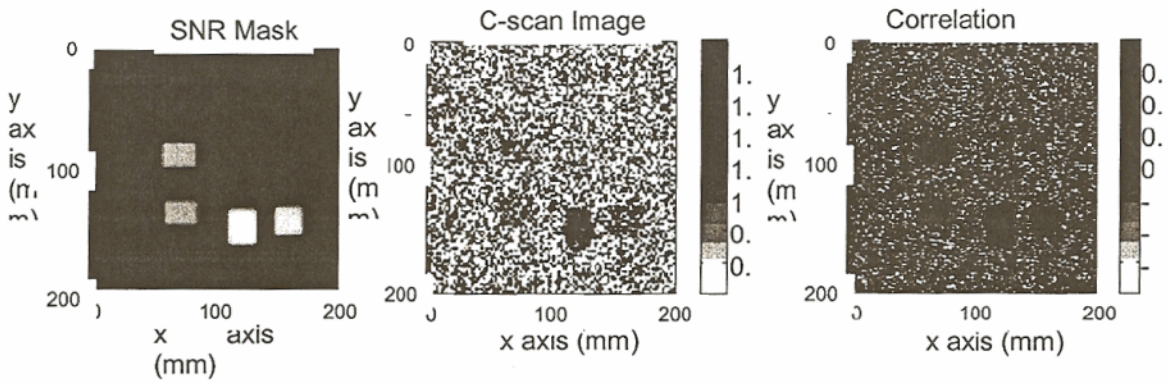

FIGURE 6. Example simulation results.

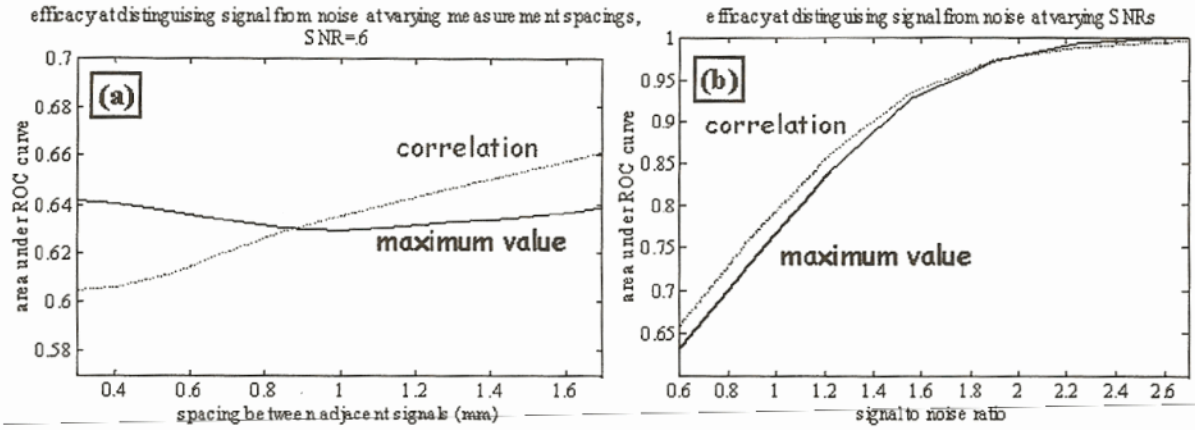

FIGURE 7. Area under the ROC curve for varying measurement spacing and SNR.

is slightly more effective than the classical C-scan approach. Additional ROC analysis is underway to consider the influence of averaging window size, defects signal distortion, and defect size on detection performance.

SUMMARY AND DISCUSSION

The results presented in this paper show that the correlation approach is a viable defect detection approach. Correlation images are easily generated and interpreted since they are based on the same A-scans used to generate C-scan images and have the same basic appearance as C-scan images. The correlation approach is an attractive scale-independent compliment to the peak-amplitude based C-scan approach and is potentially more robust at low SNR due to its reliance on signal shape rather than a single peak value.

Further development of the correlation approach is underway. Additional ROC analysis is being done to further guide decisions related to implementation of the correlation approach and to compare the correlation approach to matched filtering for different levels of defect signal distortion. More in-depth study will also be done to assess the influence of the material sample and measurement system on the correlation approach. Finally, more sophisticated detection schemes will be applied to both C-scan and correlation images to aid in the detection of low SNR defect signals.

ACKNOWLEDGMENTS

This work was supported in part by the Center for Aerospace Manufacturing Technology (CAMT) at the University of Missouri-Rolla funded under Air Force Research Laboratory Contract FA8650-04-C-5704 and by Boeing under PO Z40791. Previous support for development of the correlation approach was provided by Honeywell Federal Manufacturing and Technology and by the National Science Foundation (NSF CMS 9610189). The authors would like to acknowledge early development work on correlation analysis by Dr. Mark D. Russell while a post-doc at the University of Missouri-Columbia. The authors would also like to acknowledge the tremendous support from personnel at Honeywell FM&T including Eric Jamieson, Jose A. Samayoa, and Jason P. Miller. In particular, the encouragement by Eric Jamieson to extend the correlation approach to localized flaw detection was pivotal. Many thanks are also due to Dr. Zoughi from the University of Missouri-Rolla (UMR) for his administrative role in CAMT.

REFERENCES

1. A. Dogandzic and N. Eua-Anant, "Defect detection in correlated noise," in *Review of Progress in Quantitative Nondestructive Evaluation 23A*, edited by D. E. Chimenti and D. O. Thompson, AIP Conference Proceedings vol. 760, AIP, Melville, 2004, pp. 628-635.
2. R. B. Thompson, L. Yu, and F. J. Margetan, "A formal theory for the spatial correlation of backscattered ultrasonic grain noise," in *Review of Progress in Quantitative Nondestructive Evaluation 24B*, edited by D. E. Chimenti and D. O. Thompson, AIP Conference Proceedings vol. 820, AIP, Melville, 2005, pp. 1292-1299.
3. W. F. Walker, "The significance of correlation in ultrasound signal processing," in *Proc. SPIE Vol. 4325, Medical Imaging: Ultrasonic Imaging and Signal Processing*, edited by Michael F. Insana and K. Kirk Shung, 2001, pp. 159-171.
4. F. J. Margetan, E. Nieters, L. Brasche, L. Yu, A. Degtyar, H. Wasan, M. Keller, and A. Kinney, "Fundamental Studies of Titanium Forging Materials - Engine Titanium Consortium II", FAA William J. Hughes Technical Center, Atlantic City, N. J., Report number DOT/FAA/AR-05/22 (June 2005).

J. S. Bendat and A. G. Piersol, *Engineering Applications of Correlation and Spectral Analysis*, J. Wiley, New York, 1993, pp. 46.